Electronic Supplementary Material (ESI) for Dalton Transactions.

Supporting Information

Flow-Synthesis of Carboxylate and Phosphonate Based Metal-Organic Frameworks Under Non-solvothermal Reaction Conditions

Steve Waitschat[a], Michael T. Wharmby[a,b] and Norbert Stock [a]

[a] *Institute für Anorganische Chemie, Christian-Albrechts-Universität,*
Max-Eyth-Straße 2, D 24118 Kiel, Germany
[b] *Diamond Light Source Ltd., Diamond House, Harwell Science and Innovation Campus,*
Didcot, Oxforshire, OX11 0DE, United Kingdom

Prof. Dr. Norbert Stock, Tel.: +49-431-880-1675, Fax: +49-431-880-1775,
Email: stock@ac.uni-kiel.de

Dr Michael. T Wharmby, Tel.: +44-1235-77-8327, Fax: +44-1235-778468,
Email: michael.wharmby@diamond.ac.uk

Table of Contents

S1 Previous Reports of Flow Syntheses

S2 Reagents

S3 Description of the Non-Solvothermal Flow Reactor

S4 Flow Synthesis & Characterization of UiO-66

  S4.1 Flow Reactor Synthesis

  S4.2 UiO-66: Powder Diffraction Pattern & Pawley Fit

  S4.3 UiO-66: Thermal & Elemental Analysis

  S4.4 UiO-66: Infrared Spectrum

  S4.5 UiO-66: SEM Image

  S4.6 UiO-66: N2 Sorption Experiments

S5 Flow Synthesis & Characterization of CAU-13

  S5.1 Flow Reactor Synthesis

  S5.2 CAU-13: Pawley Fit

  S5.3 CAU-13: Thermal & Elemental Analysis

  S5.4 CAU-13: Infrared Spectrum

  S5.5 CAU-13: NMR Spectrum

  S5.6 CAU-13: SEM Image

  S5.7 CAU-13: N2 Sorption Experiments

S6 Flow Synthesis & Characterization of STA-12(Cd)

  S6.1 Flow Reactor Synthesis

  S6.2 Structural Analysis of STA-12(Cd):
  Details of Rietveld refinement; Structure; Crystallographic Tables

  S6.3 STA-12(Cd): Thermal & Elemental Analysis

  S6.4 STA-12(Cd): Infrared Spectrum

  S6.5 STA-12(Cd): NMR Spectrum

  S6.5 STA-12(Cd): SEM Image

  S6.6 STA-12(Cd): N2 Sorption Experiments

S7 References

S1 Previous Reports of Flow Reactor Syntheses

Table S1.1. Summary of the published syntheses of Metal-Organic Framework (MOF) compounds in flow reactors and their reaction conditions.

Framework	Metal Source	Linker	Solvent	Temp. / °C	Time / min	Pressure / bar	Reference
HKUST-1	$Cu(NO_3)\ 2.5H_2O$	H_3BTC	$H_2O/DMF/EtOH$	100 - 400	0.0167	250	[1]
HKUST-1	$Cu(NO_3)_2\cdot 6H_2O$	H_3BTC	EtOH or H_2O	60 - 160	5	100	[2]
HKUST-1	$Cu(NO_3)_2\cdot H_2O$	H_3BTC	$DMF/EtOH/H_2O$	90	1 - 12	-	[3]
HKUST-1	$Cu(NO_3)_2\cdot H_2O$	H_3BTC	EtOH	200	15	75	[4]
HKUST-1	$Cu(NO_3)_2\cdot 3H_2O$	H_3BTC	EtOH	140	1 - 10	≤ 20	[5]
CPO-27(Ni)	$Ni(AcO)_2\cdot 4H_2O$	H_2DOBDC	H_2O/DMF	200	0.0167	205	[1]
MIL-88B(Fe)	$FeCl_3\cdot 6H_2O$	H_2BDC	DMF/H_2O	95	4	-	[6]
MIL-53(Al)	$Al(NO_3)_3\cdot 9H_2O$	H_2BDC	H_2O	250	20	230	[4]
UiO-66	$ZrCl_4$	H_2BDC	DMF/HCl	140	15	-	[3]
UiO-66	$ZrCl_4$	H_2BDC	DMF	130	10	≤ 20	[5]
UiO-66	$ZrCl_4$	H_2BDC	DMF	120	45	-	This work
UiO-66-NH_2	$ZrCl_4$	H_2BDC-NH_2	DMF	100-120	720	-	[7]
NOTT-400	$Sc(SO_3CF_3)_3$	H_4BPTC	$DMF/THF/H_2O$	85	15	≤ 20	[5]
MOF-5	$Zn(NO_3)6\cdot H_2O$	H_2BDC	DMF	120	3	-	[3]
IRMOF-3	$Zn(NO_3)\ 6H_2O$	H_2BDC-NH_2	DMF	120	3	-	[3]
$[Ce_5(BDC)_{7.5}(DMF)_4]$	$Ce(NH_4)_2(NO_3)_6$	H_2BDC	DMF	230	0.5	100	[8]
CAU-13	$AlCl_3\cdot 6H_2O$	H_2CDC	DMF/AcOH	130	20	-	This work
STA-12(Cd)	$Cd(AcO)_2\cdot 2H_2O$	H_4L	H_2O/KOH	70	15	-	This work

* H_3BTC – Benzene-1,3,5-tricarboxylic acid; H_2BDC – Benzene-1,4-dicarboxylic acid; H_2BDC-NH_2 – 2-aminobenzene-1,4-dicarboxylic acid; H_2DOBDC – 2,5-dihydroxybenzene-1,4-dicarboxylic acid; H_4BPTC – Biphenyl-3,3',5,5'-tetracarboxylic acid; H_2CDC – Cyclohexane-1,4-dicarboxylic acid; H_4L – N,N'-piperazinebis(methylenephosphonic acid).

S2 Reagents

Table S2.1. List of reagents and suppliers used in the synthesis of inorganic-organic hybrid compounds in the flow reactor

Reagent	Supplier	Reagent	Supplier
Aluminium(III) chloride hexahydrate	Sigma Aldrich	*trans*-1,4-cyclohexane-dicarboxylic acid	ABCR
Cadmium acetate dihydrate	ABCR	1,4-benzenedicarboxylic acid	Sigma Aldrich
Cobalt(II) acetate tetrahydrate	ABCR	Acetic acid	Alfa Aesar
Nickel(II) acetate terahydrate	Alfa Aesar	N,N-dimethylformamide (DMF)	BASF
Zirconium tetrachloride	ABCR	Paraffin	Alfa Aesar
		Potassium hydroxide (pellets)	BAK

N,N'-piperazinebis(methylenephosphonic acid) (H_4**L**) was synthesised following the method reported by Mowat *et al.*[9]

Table S2.2. List of reagents and suppliers used in the synthesis of the linker H_4**L**.

Reagent	Supplier	Reagent	Supplier
Piperazine	Alfa Aesar	Phosphorous acid	ABCR
Formaldehyde	Alfa Aesar	Hydrochloric acid	Alfa Aesar

S3 Description of the Non-Solvothermal Flow Reactor

Two configurations of the non-solvothermal flow reactor reported in this work were developed: the first with three syringe pumps (two reagents and one transport medium); the second with two syringe pumps (two reagents) and fitted with an ultrasonic probe. Both configurations are assembled from widely available commodity hardware (Table S3.1).

Table S3.1. List of parts & materials used to assemble the flow reactor.

Part	Supplier	Part	Supplier
Syringe pump LA-100	Landgraf Laborsysteme HLL GmbH, Germany	Teflon® tube (ID = 1.6 mm)	Eydam KG, Germany
PEEK/PTFE Y- and X-connectors	TechLab GmbH, Germany	Flangeless Ferules and nuts	Upchurch Scientific, IDEX Health & Science LLC, USA
Stirrer Hotplate	Eydam KG, Germany	Ultrasonic Probe UP-200s	Dr. Hielscher GmbH, Germany

Figure S3.1. Photograph of the two syringe pump configuration of the flow reactor including the ultrasonic probe (centre).

In both configurations, solutions of reagents are loaded into syringe pumps. These are then connected through lengths of Teflon® tube to a three-way Y- or four-way X-connector (for the three & four pump configurations respectively). At this point, the two reagents in the system first mix together. In the three-pump configuration, in addition to the two reagent flows, a transport flow is also pumped into the X-connector, which helps to prevent clogging by either increasing the flow rate (when solvents are used as the transport medium) or by forming bubbles of reagent solution (when paraffin is used) which are isolated from each other and also from the walls of the reactor tube. The molar ratio of reagents mixing in the reactor is a function of the concentrations of the solutions and their relative pumping rates (Eq.S3.1). The residence time of the reagents in the reactor is a function of the total volume of the reactor (V_Σ) and the overall flow rate (Eq.S3.2).

$$mol_n = M_n * 1000 * f_n$$

Equation S3.1. The amount of the nth reagent in the flow reactor (mol_n in mol min^{-1}) is calculated from the concentration (M_n in mol dm^{-3}) and the flow rate (f_n in ml min^{-1}).

$$t = \frac{V_\Sigma}{\sum_n f_n}$$

Equation S3.2. Residence time in the flow reactor (t in min) determined by the sum of all flow rates (f_n in ml min^{-1}) and the volume of the flow reactor (V_Σ in ml).

S4 Flow Synthesis and Characterisation of UiO-66

S4.1 Flow Reactor Synthesis

For the flow reactor syntheses, zirconium tetrachloride ($ZrCl_4$) and the linker 1,4-benzenedicarboxylic acid (terephthalic acid, H_2BDC) were dissolved in N,N-dimethylformamide (DMF) to yield two solutions both with concentrations of 0.1 mol dm^{-3}. These solutions were then loaded into the syringe pumps and connected to the flow reactor with either two- or three-pump configurations. Typical syntheses in both these configurations are given below.

S4.1.1 Typical Three-Pump Configuration

The loaded syringe pumps were connected into a three syringe pump configuration (metal, linker and paraffin) and solutions were injected into a flow reactor (V_Σ = 14.45 ml) with flow rates of 0.040 ml min^{-1}, 0.120 ml min^{-1} and 0.161 ml min^{-1} for the metal, linker and paraffin respectively, giving amolar ratio of reagents of 1:3 ($ZrCl_4$:H_2BDC) total reaction time of 45 mins. During the reaction the flow reactor was kept at a temperature of 120°C. The reaction product was collected, and separated by filtration and washed sequentially with dichloromethane (DCM) and ethanol.

S4.1.2 Typical Two-Pump Configuration

The loaded syringe pumps were connected into a two syringe pump configuration (metal and linker) fitted with a ultrasonic probe to prevent clogging. The solutions were injected into a flow reactor (V_Σ = 16.87 ml) with flow rates of 0.094 ml min^{-1} and 0.281 ml min^{-1} for the metal and linker solutions respectively, giving a total reaction time of 45 mins. During the reaction the flow reactor was kept at a temperature of 120°C and the ultrasonic probe was set up with a cycle of 0.25 and amplitude of 100 %. The product was collected, and separated by centrifugation and washing with DMF followed by ethanol.

S4.1.3 Summary of Flow Reactor Experiments

Table S4.1. Summary of the reaction conditions tested for the synthesis of UiO-66 using the flow reactor.

V_Σ / ml	$ZrCl_4$ Flowrate / ml min^{-1}	H_2BDC Flowrate / ml min^{-1}	Transport[a] Flowrate / ml min^{-1}	Temp. / °C	Time / min	Ultra Sound	
						Cycle	Amplitude
14.45	0.040	0.120	0.161 (Para.)	120	45	-	-
16.83	0.047	0.140	0.187 (DMF)	130	45	-	-
16.87[b]	0.094	0.281	-	120	45	0.25	100 %
16.80	0.070	0.210	-	120	60	0.25	100 %
16.87	0.094	0.281	-	120	45	-	-
16.80	0.070	0.210	-	120	60	-	-

[a] A transport medium in addition to the reaction solvent, used to prevent clogging of the reactor.

[b] This reaction produced the most crystalline and phase pure UiO-66, which is further analysed in this work. This is equivalent to a reaction ratio of 1:3 ($ZrCl_4$:H_2BDC).

Table S4.2. Optimised reaction conditions for the synthesis of UiO-66 using the a three-pump flow reactor, with paraffin as the transport medium, and a two-pump flow reactor fitted with an ultrasonic probe (cycle 0.25, amplitude 100 %).

	$ZrCl_4$ Flowrate / ml min^{-1}	**H_2BDC Flowrate / ml min^{-1}**	**Transport Flowrate / ml min^{-1}**	**Temp. / °C**	**Time**
Three-pump	0.040	0.120	0.161	120	45
Two-pump	0.094	0.281	-	120	45

S4.2 UiO-66: Powder Diffraction Pattern & Pawley Fit

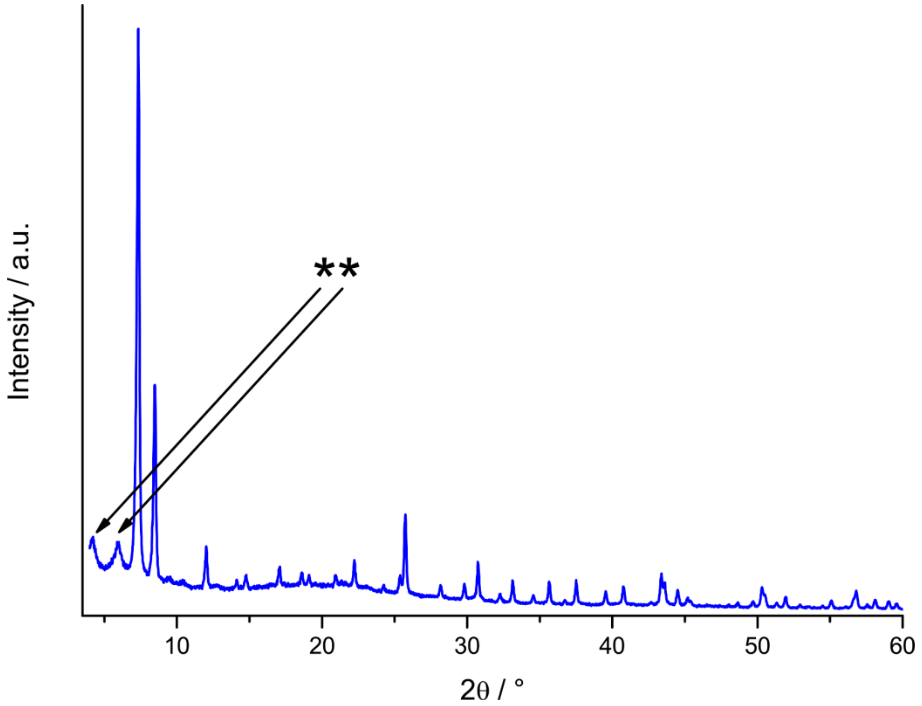

Figure S4.1. PXRD pattern of UiO-66 produced in the flow reactor (λ = Cu $K_{\alpha1}$). The asterisks indicate two symmetry forbidden reflections, which indicate defect rich regions within the sample.[10]

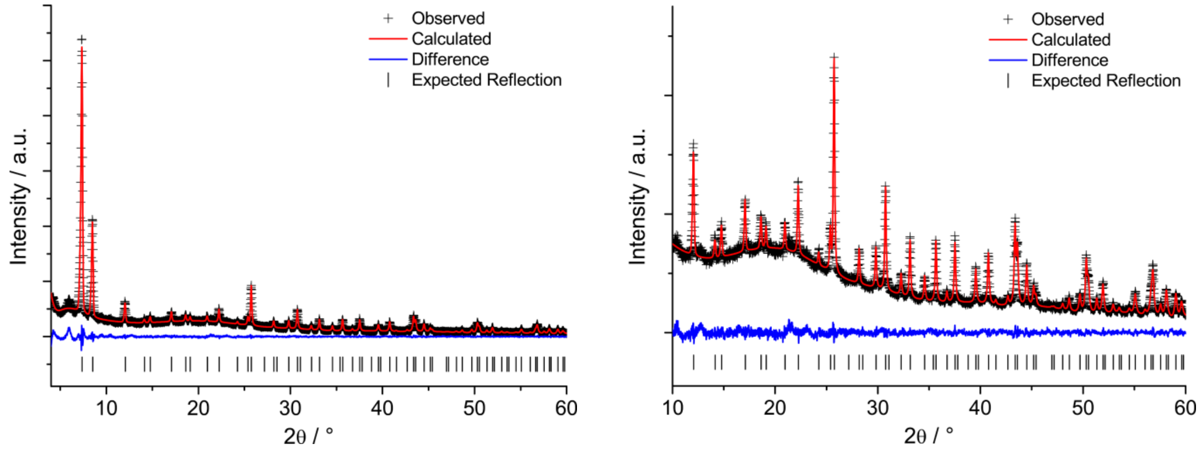

Figure S4.2. Pawley fit of UiO-66 (λ = Cu $K_{\alpha1}$), showing the range from 4-60° 2θ (left) and 10-60° 2θ (right). Final fit to a cubic unit cell in space group $Fm\bar{3}m$, with the unit cell parameter a = 20.7367(4) Å. (R_{wp} = 5.59 %, χ^2 = 3.644). The determined cell parameter is very similar to the literature value of a = 20.7751(2) Å.[11]

S4.3 UiO-66: Thermal & Elemental Analysis

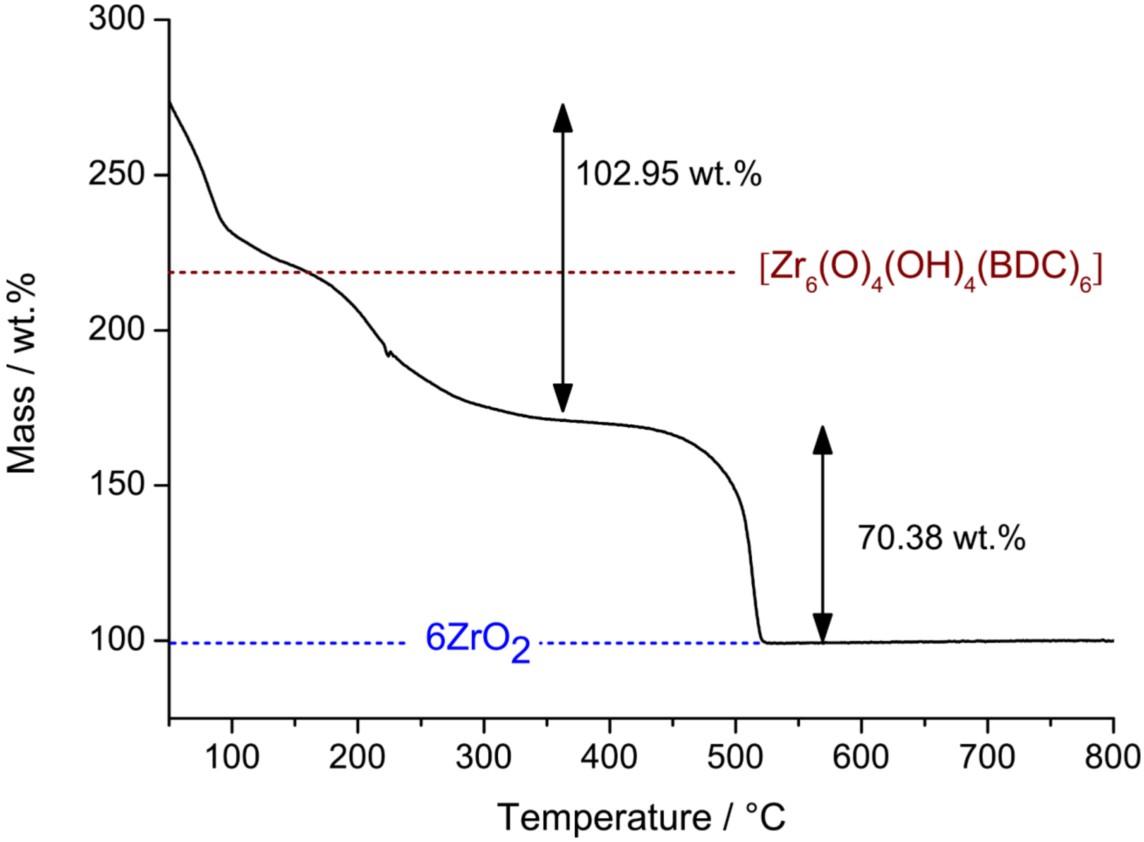

Figure S4.3. TGA plot for UiO-66 produced in the flow reactor. The principal weight loss events are indicated, assigned to the loss of solvent molecules (DMF, ethanol water) from the pores and to the collapse of the framework, to yield ZrO_2 as the final product (70.38 wt.%; expected 120 wt.%). The red dashed line represents the expected fractional mass of $[Zr_6O_6(BDC)_6]$, calculated from ZrO_2 (blue dashed line); the large difference between expected and observed weight losses indicates there are significant numbers of missing BDC^{2-} linkers.[12]

Table S4.3. Elemental analysis of UiO-66 obtained from the flow reactor compared to the expected values for $[Zr_6O_4(OH)_4(BDC)_6]$. It was not possible to identify the exact amount of DMF in the pores and thus there is a large discrepancy in the measured and calculated elemental analysis values.

	C %	H %	N %	S %
Found	27.5	3.2	4.4	0
Expected[a]	34.6	1.7	0	0

[a] Calculated for $[Zr_6O_4(OH)_4(BDC)_6]$.

EDX measurements indicate the presence of chlorine in the sample (assumed to be Cl^- ions, in ratios with Zr^{4+} of between 1:1 and 2:1 (Cl^-:Zr^{4+}), which is consistent with the presence of defect regions within the framework.[12]

S4.4 UiO-66: Infrared Spectrum

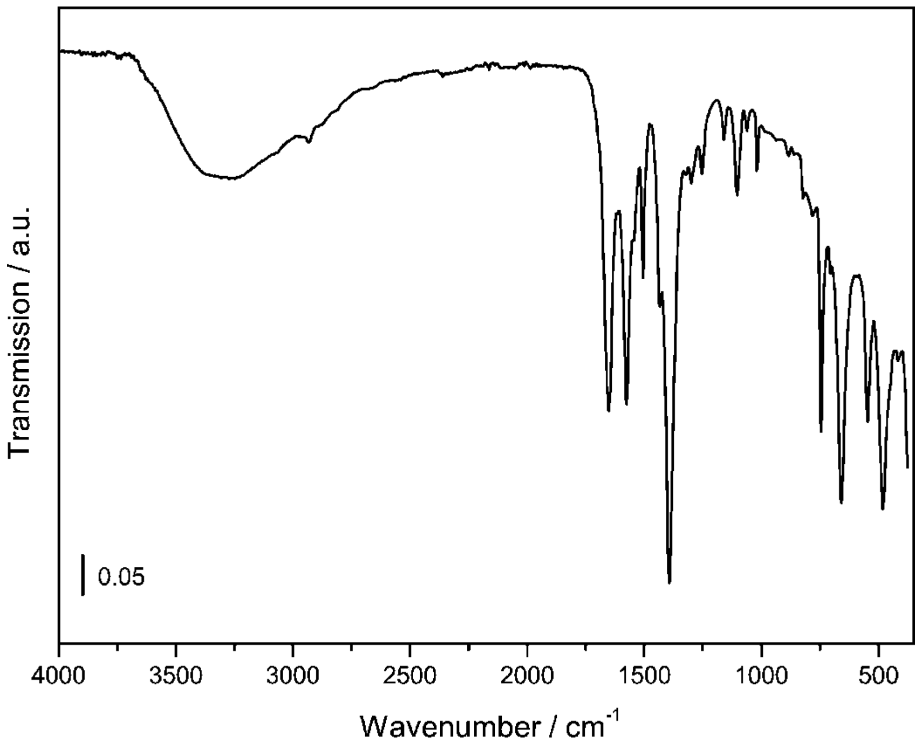

Figure S4.4. FTIR spectrum of UiO-66. $\tilde{\nu}$ (cm-1) = 3348 (b, O-H stretch – H_2O), 1659 (m, C-O stretch – DMF), 1573 (m, asymmetric CO_2^- stretch – BDC^{2-}), 1393 (s, symmetric CO_2^- stretch – BDC^{2-}).

S4.5 UiO-66: SEM Image

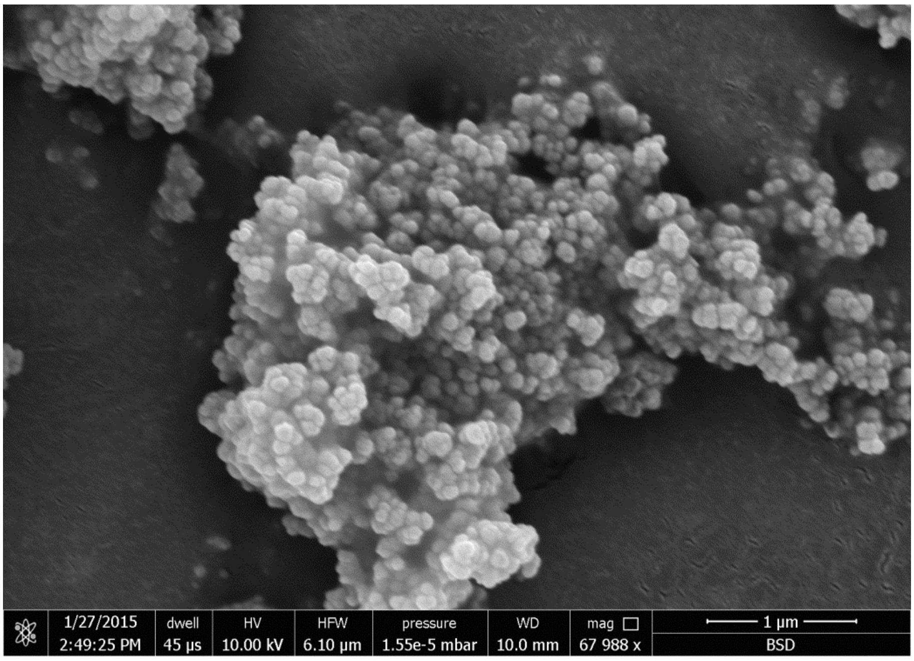

Figure S4.5. SEM micrograph of UiO-66 sample produced in the flow reactor. Particles appear to have the shape of small spheres, approximately 100 nm across. The size distribution of the particles is also quite small.

S4.6 UiO-66: N_2 Sorption Experiments

For sorption experiments, UiO-66 was activated by heating the sample to 220°C under dynamic vacuum overnight. Samples from both a three-pump configuration (where paraffin was used as the transport medium) and a two-pump configuration (using the ultrasonic probe) were investigated and both found to be porous though to different degrees (Fig S4.6).

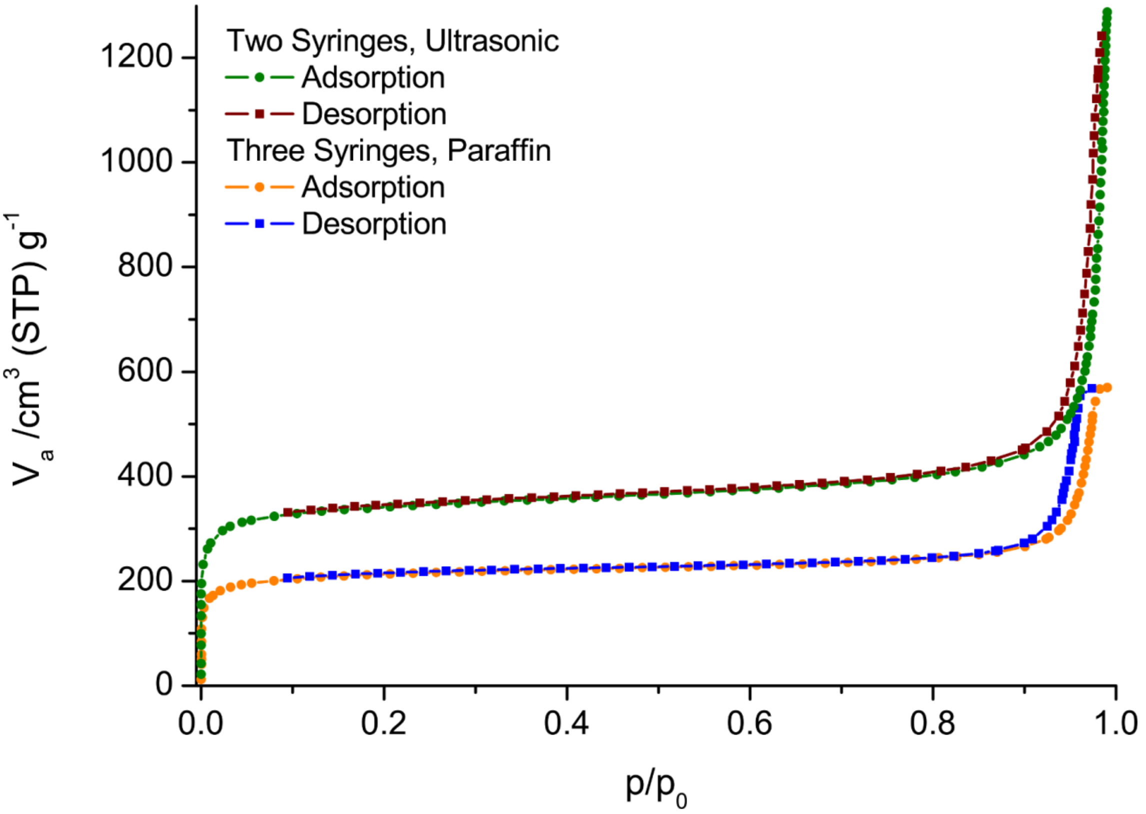

Figure S4.6. N_2 adsorption and desorption isotherms measured at 77 K on samples of UiO-66 produced in a two-pump (ultrasonic probe; green & red traces) and three-pump (paraffin transport; orange & blue traces) flow reactor.

Table S4.4. BET surface areas and micropore volumes for UiO-66 samples produced using the two-pump (ultrasonic probe) and three-pump (paraffin transport) configurations of the flow reactor.

Flow Reactor Configuration	**BET / m^2 g^{-1}**	**Micropore Volume / cm^3 g$^{=1}$**
Two-pumps	1263(8)	0.54
Three-pumps	786(5)	0.33

The ideal surface area for a perfect sample of UiO-66 has been calculated as 1125 m^2 g^{-1}.[12] PXRD, TGA, elemental analysis and EDX measurements have indicated that our samples of UiO-66 contain a significant density of defects and thus it is expected that they will show significantly larger surface areas than this ideal value. The three-pump product shows a significantly lower surface area however, which is attributed to the inclusion of residual and hard to remove paraffin within the pore spaces. By comparison, the sample produced from the two-syringe reactor has a BET surface area slightly higher than the expected ideal value. This result is consistent with the presence of defects and is expected.

The sensitivity of the UiO-66 samples to the activation procedure was also investigated. The PXRD patterns of the UiO-66 sample from the two-pump reactor were collected before and after the adsorption experiment. These indicate no significant degradation of the structure on activation (Fig. S4.7).

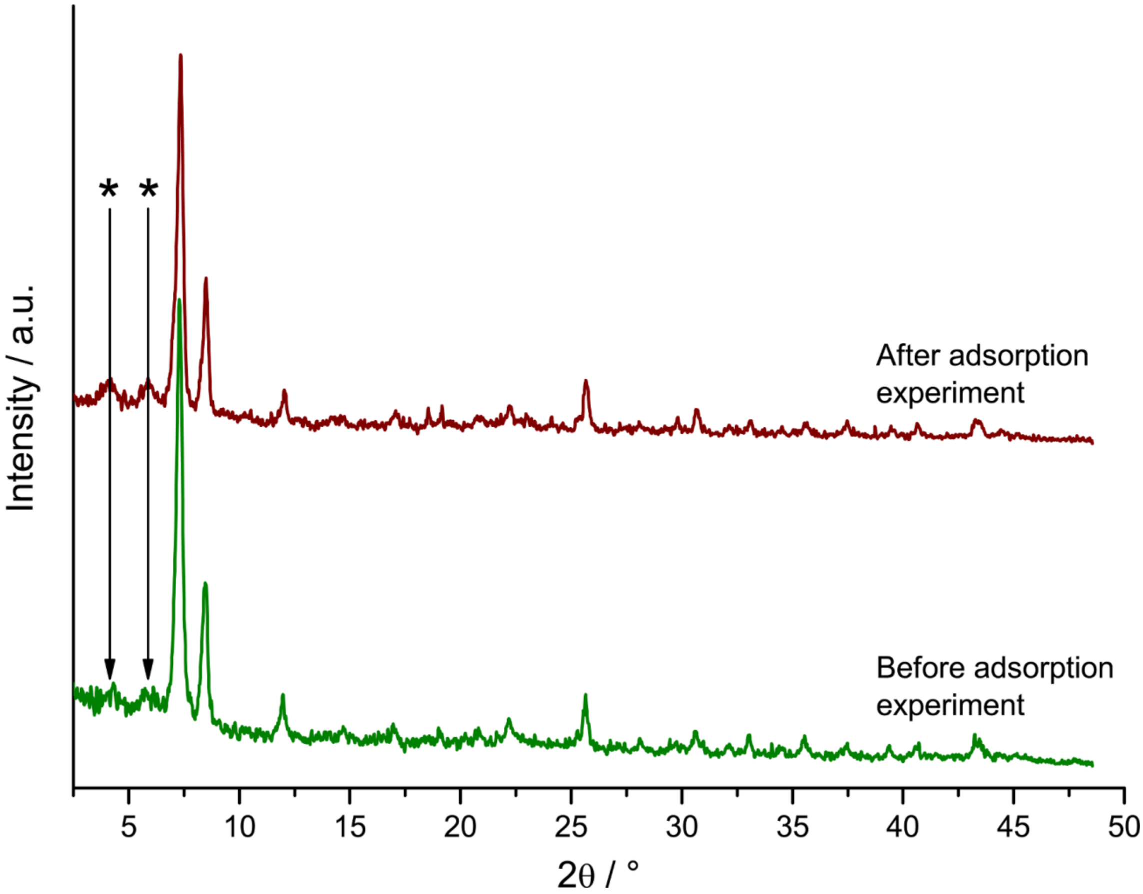

Figure S4.7. PXRD patterns (λ = Cu $K_{\alpha1}$) of UiO-66 produced using the two-pump reactor configuration, before and after activation for the N_2 sorption experiment. *s indicate the symmetry forbidden reflections attributed to defect rich regions of the sample.

S5 Flow Synthesis & Characterisation of CAU-13

S5.1 Flow Reactor Synthesis

For flow reactor syntheses, aluminium(III) chloride hexahydrate ($AlCl_3 \cdot 6H_2O$) was dissolved in DMF to yield a 0.5 mol dm^{-3} solution and loaded into a syringe pump. A second syringe pump was charged with a 0.5 mol dm^{-3} solution of the linker, *trans*-1,4,-cyclohexanedicarboxylic acid (*trans*-H_2CDC). To this was added acetic acid (AcOH) to give a final ratio of H_2CDC: AcOH of 1:9. AcOH was used to act as modulator in synthesis.[13]

S5.1.1 Typical Two-Pump Synthesis

The loaded syringe pumps were connected into a two syringe pump configuration (metal, linker:AcOH) and injected into a flow reactor (V_Σ = 16.16 ml) with equal flow rate for each pump of 0.404 ml min^{-1}, giving a molar ratio of the reagents of 1:1 ($AlCl_3$:H_2CDC) and a total reaction time of 20 mins. During the reaction the flow reactor was kept at a temperature of 130°C. The product was collected and the solid separated by sequential centrifugation and washing with DMF followed by ethanol.

S5.1.2 Summary of Flow Reactor Experiments

Table S5.1. Summary of reaction conditions tested for the synthesis of CAU-13 using the flow reactor.

V_Σ / mL	$AlCl_3$ Flowrate / ml min^{-1}	H_2CDC Flowrate / ml min^{-1}	Transport[a] Flowrate / ml min^{-1}	Conc.[b] / mol dm^{-3}	AcOH:H_2CDC Ratio	Temp. / °C	Time / min
15.25	0.381	0.381	-	0.1	-	120	20
15.25	0.381	0.381	-	0.1	1:9	120	20
15.25	0.381	0.381	-	0.1	1:9	130	20
15.25	0.381	0.381	-	0.1	1:9	140	20
15.25	0.190	0.190	0.381	0.1	1:9	130	20
15.25	0.127	0.127	0.254	0.1	1:9	130	30
15.25	0.085	0.085	0.169	0.1	1:9	130	45
15.25	0.127	0.254	0.381	0.1	1:9	130	20
15.25	0.085	0.169	0.245	0.1	1:9	130	30
15.25	0.056	0.113	0.169	0.1	1:9	130	45
16.16[c]	0.404	0.404	-	0.5	1:9	130	20
16.16	0.269	0.269	-	0.5	1:9	130	30
16.16	0.179	0.359	-	0.5	1:9	130	30
16.84	0.421	0.421	-	0.5	1:9	130	20

[a] A transport medium in addition to the reaction solvent, used to prevent clogging of the reactor, in this case DMF.

[b] The concentration of the reagent solutions was also investigated, with both syringe pumps have the same concentration.

[c] This reaction produced the most crystalline and phase pure CAU-13, which is further analysed in this work. This is equivalent to a reaction ratio of 1:1 ($AlCl_3$:H_2CDC).

Table S5.2. Optimised reaction conditions for the synthesis of CAU-13 using the flow reactor.

$AlCl_3$ Flowrate / ml min^{-1}	H_2CDC/AcOH Flowrate / ml min^{-1}	H_2CDC:AcOH	Temperature / °C	Time / min
0.404	0.404	1:9	130	20

S5.2 CAU-13: Pawley Fit

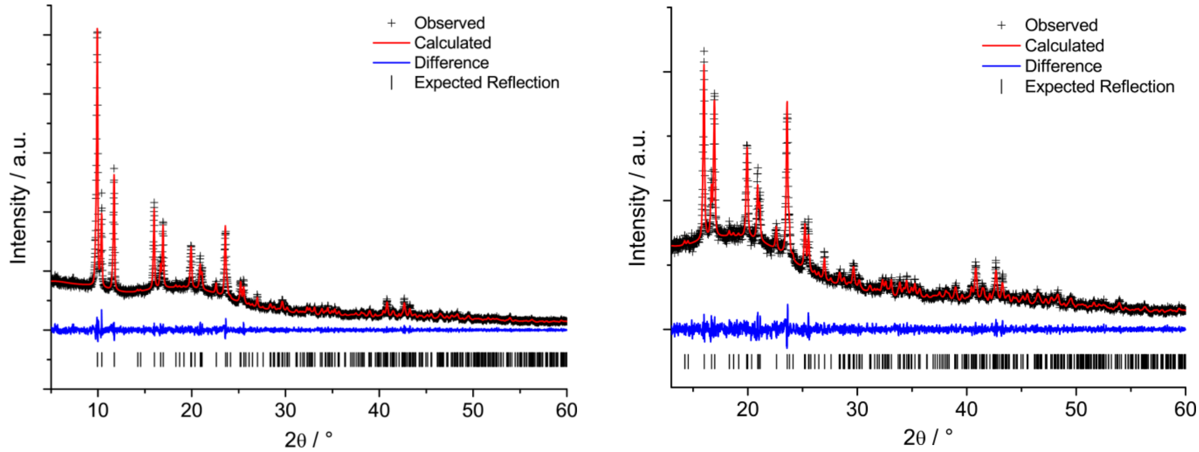

Figure S5.1. Pawley fit of CAU-13 (λ = Cu $K_{\alpha 1}$), showing the range from 4-60° 2θ (left) and 13-60° 2θ (right). Final fit to a triclinic unit cell in space group $P\bar{1}$, with unit cell parameters a = 6.6111(4) Å, b = 9.4498(6) Å, c = 9.4652(5) Å, α = 107.652(4)°, β = 107.690(6)° and γ = 93.185(5)°. (R_{wp} = 4.71 %, χ^2 = 1.080). The determined cell parameters are very similar to the literature parameters of a = 6.6169(5) Å, b = 9.4300(6) Å, c = 9.4642(6) Å, α = 107.577(3)°, β = 107.725(7)° and γ = 93.209(5)°.[14]

S5.3 CAU-13: Thermal & Elemental Analysis

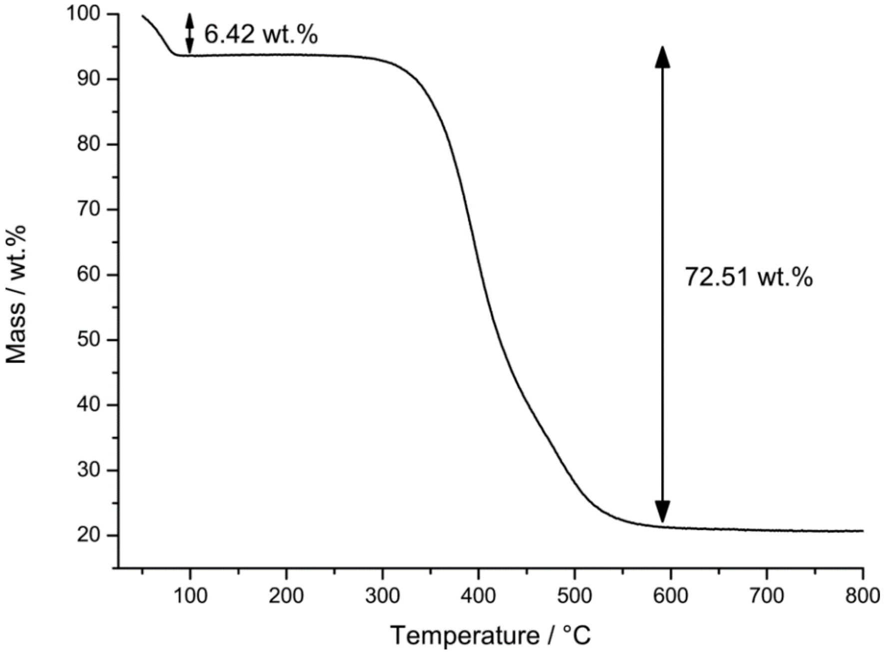

Figure S5.2. TGA plot for CAU-13 produced in the flow reactor. The principal weight loss events are indicated, assigned to the loss of one molecule of H_2O per formula unit from the structure (6.42 wt.%; expected 7.76 wt.%) and collapse of the framework to form Al_2O_3 (72.51 wt.%; expected 70.28 wt.%).

Table S5.3. Elemental analysis of CAU-13 obtained by flow synthesis with the theoretical one ([Al(OH)($C_8H_{10}O_4$)]·H_2O). The small amount of N found in the flow reactor product is attributed to residual DMF in the structure and this may also account for the discrepancies in the amounts of C and H in the sample.

	C %	H %	N %	S %
Found	40.1	6.2	0.1	0
Expected	41.4	5.6	0.0	0

S5.4 CAU-13: Infrared Spectrum

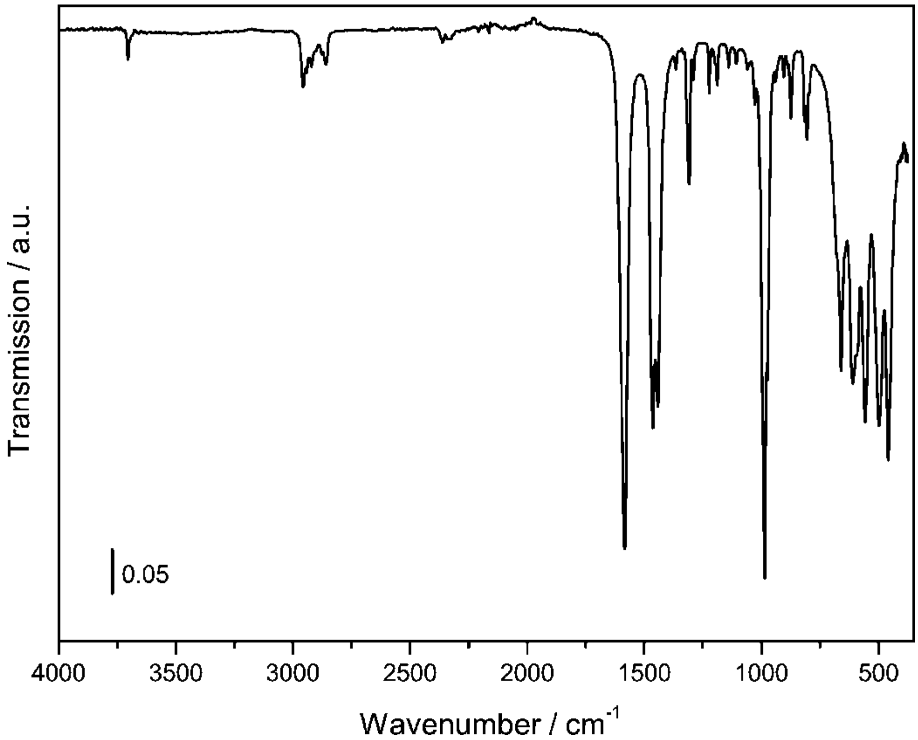

Figure S5.3. FTIR spectrum of CAU-13. ṽ (cm^{-1}) = 3704 (m, O-H stretch), 2955 (m, asymmetric C-H stretch – cdc^{2-}), 2842 (m, symmetric C-H stretch – cdc^{2-}), 1587 (s, asymmetric CO_2^- stretch – cdc^{2-}), 1456 (s, symmetric CO_2^- stretch – cdc^{2-}), 983 (s, C-C stretch, cdc^{2-}).

S5.5 CAU-13: NMR Spectrum

A sample of CAU-13 was digested for solution state NMR analysis using a NaOD/D_2O solution. The spectrum (Fig. S5.4) shows a strong resonance for water ($\delta = 4.93$ ppm) and several much lower intensity overlapping resonances in the region 0 – 2 ppm (Fig. S5.4 inset). By comparison with an NMR spectrum of the H_2CDC linker, dissolved in a similar NaOD/D_2O solution, it is clear that the only organic present is the H_2CDC and therefore no acetic acid/acetate anions have been incorporated into the structure.

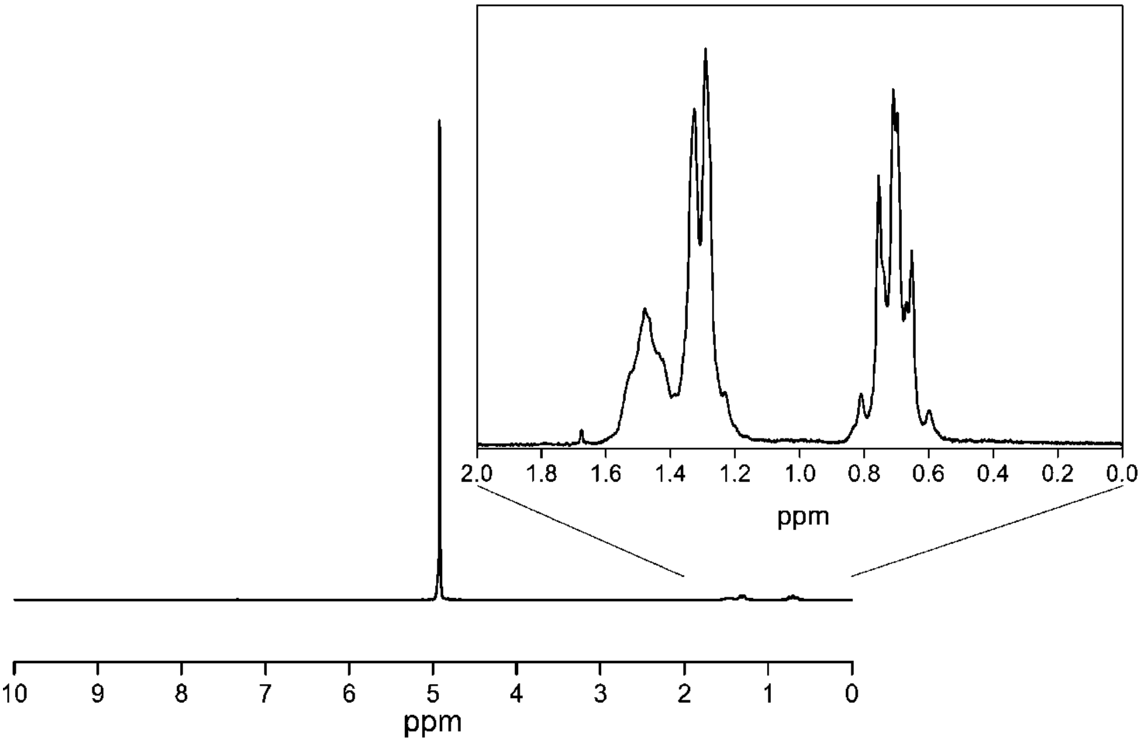

Figure S5.4. Solution state NMR spectrum of CAU-13 obtained from the flow reactor in a NaOD/D_2O solution. Inset shows an enlarged view of the region 0 – 2 ppm.

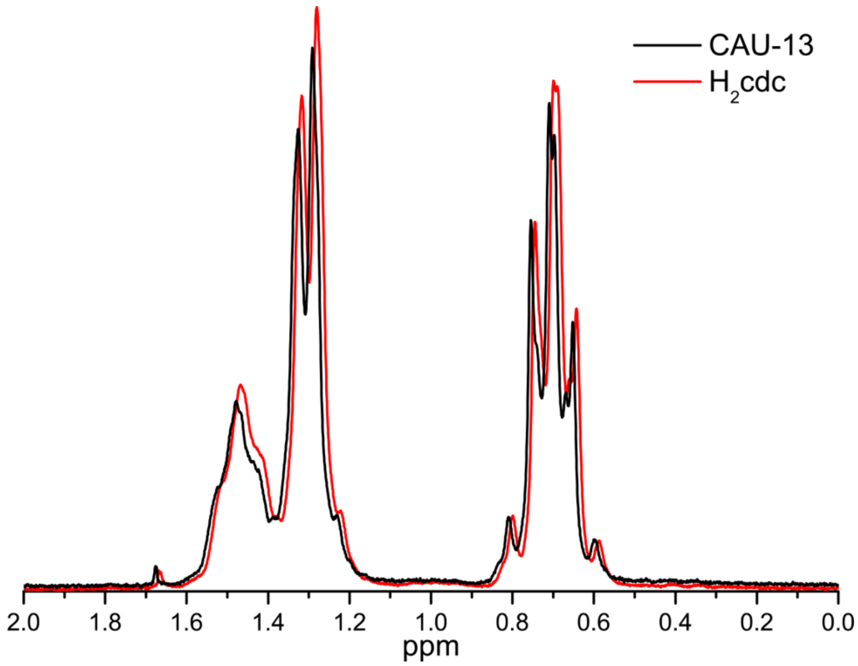

Figure S5.5. Solution state NMR spectra of CAU-13 (black) and linker H_2cdc (red) in the region 0 – 2 ppm. Both spectra were measured in NaOD/D_2O.

S5.6 CAU-13: SEM Image

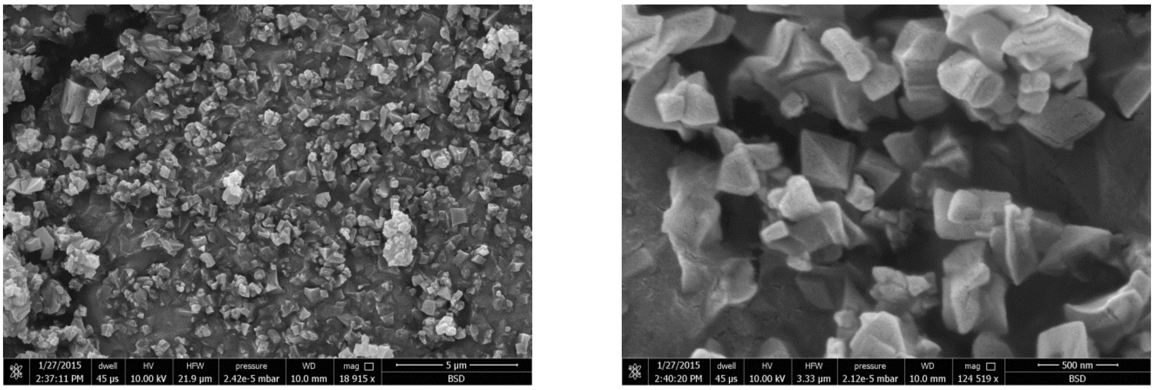

Figure S5.6. SEM micrographs of CAU-13 produced with the flow reactor. The image on the right is a higher magnification view of some of the crystals in the field of view of the left hand micrograph. Crystallites at both magnifications exhibit a blocky form, but show no regular shape. At higher magnification it is clear that there is a large distribution of crystallite sizes in the sample.

S5.7 CAU-13: N_2 Sorption Experiments

CAU-13 was activated for sorption measurements by heating the sample to 200°C under dynamic vacuum for 12 hrs. CAU-13 is porous to N_2 at 77 K (Fig. S5.7) and has a BET surface area of 401(6) $m^2\,g^{-1}$ (calculated over the range $p/p_0 = 0.037\text{-}0.183$) and a micropore volume of 0.18 $m^2\,g^{-1}$ (calculated by the Dubinin-Radushkevitch – D-R – method).[15] These values are slightly higher than those previously reported for CAU-13, but within reasonable sample-to-sample variation (literature: BET – 378 $m^2\,g^{-1}$; micropore volume – 0.15 $cm^3\,g^{-1}$).[14]

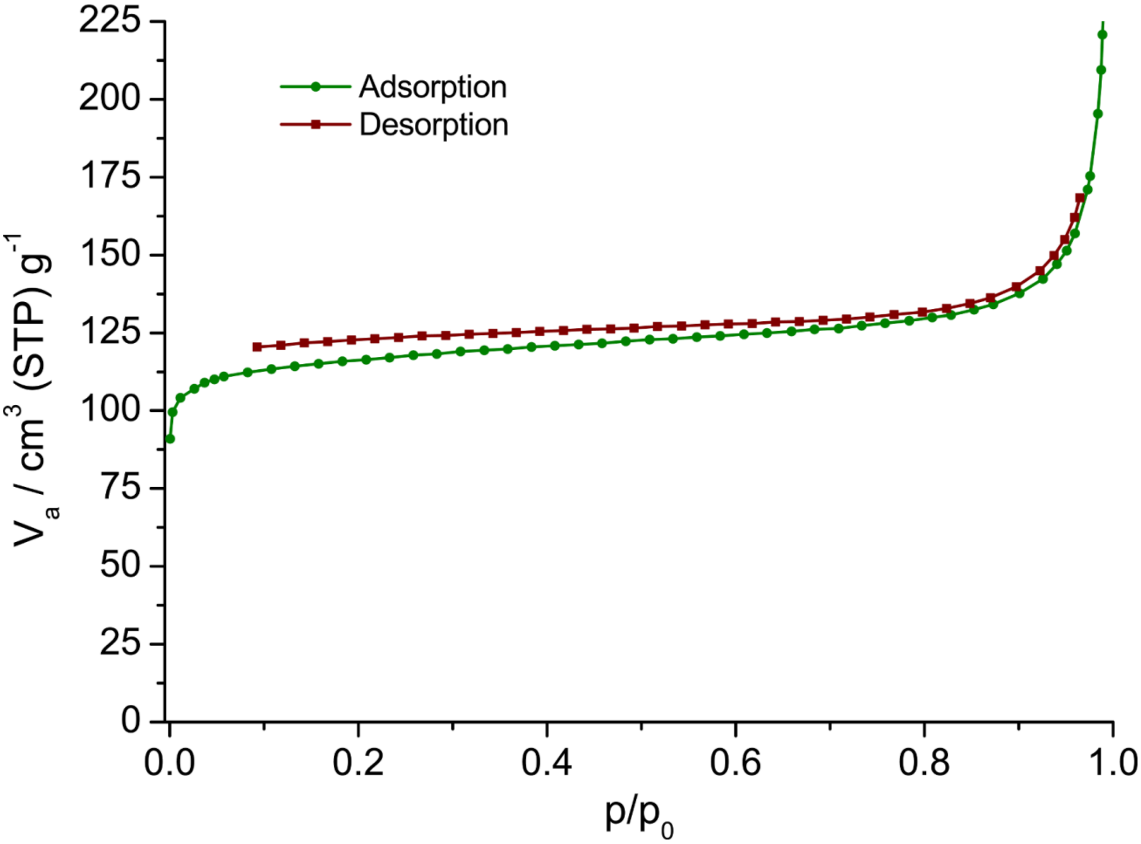

Figure S5.7. N_2 adsorption and desorption isotherms for CAU-13, measured at 77 K.

PXRD patterns were collected before and after the activation procedure to confirm that the crystallinity of the sample was unaffected by heating under vacuum (Fig. S.8), although differences were observed due to the flexible nature of the framework.

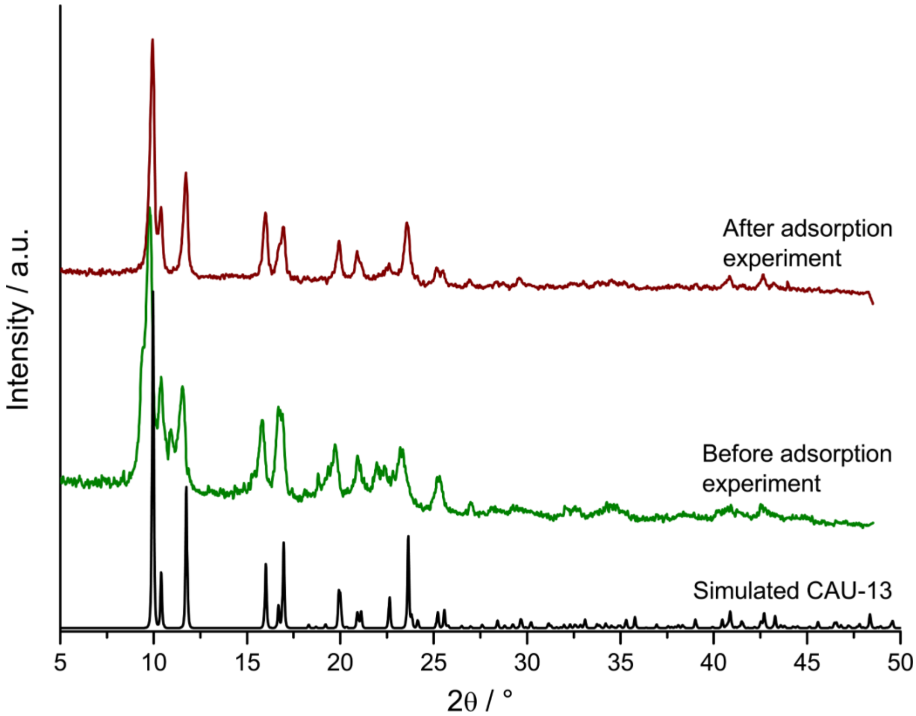

Figure S5.8. PXRD patterns (λ = Cu K$_{\alpha1}$) for CAU-13 before and after activation for the N_2 sorption experiment and the theoretical PXRD pattern for CAU-13.[14] The difference in the PXRD pattern is caused by the flexible nature of the framework, which undergoes a breathing transition an adsorption/desorption of guest molecules.

S6 Flow Synthesis & Characterisation of Reported STA-12 Frameworks and New Compound STA-12(Cd)

S6.1 Flow Reactor Synthesis

Initial work on the STA-12 family of compounds focused on the preparation of the known Ni^{2+} and Co^{2+} compounds,[16,17] whilst subsequently a new member of this family of compounds, STA-12(Cd) was prepared. In the initial work, 0.1 mol dm^{-3} aqueous solutions of nickel(II) acetate or cobalt(II) acetate were prepared and loaded into a syringe pump which was then connected to a three-pump configured flow reactor. For the synthesis of STA-12(Cd), a 0.1 mol dm^{-3} aqueous solution of cadmium(II) acetate was used as the metal source and a two-pump set up was employed.

In all reactions, due to the insolubility of the linker, N,N'-piperazinebis(methylenephosphonic acid) ($H_4\mathbf{L}$), in water below 120°C, a 0.1 mol dm^{-3} solution of the potassium salt of the linker was formed, dissolving solid $H_4\mathbf{L}$ in a solution of potassium hydroxide, in a molar ratio of 1:2 ($H_4\mathbf{L}$:KOH). This solution was then loaded into a syringe pump and connected to the flow reactor in a three-pump configuration, using paraffin as the transport medium.

S6.1.1 Preliminary Studies – Typical Synthesis

The loaded syringe pumps were connected to a flow reactor (V_Σ = 14.80 ml) and the solutions were injected with flow rates of 0.987 ml min^{-1} : 0.493 ml min^{-1} : 1.48 ml min^{-1} (metal : $H_4\mathbf{L}$/KOH : paraffin), to give a molar ratio of reagents of 2:1 (M^{2+}:$H_4\mathbf{L}$), as reported in the literature, and a reaction time of 5 min. Products were collected and paraffin was removed by sequential centrifugation and washing with toluene. The products were isolated by a further sequence of centrifugation and washing with ethanol.

S6.1.2 Preliminary Studies – Flow Reactor Experiments

Table S6.1. Summary of conditions tested for the synthesis of STA-12(Co) using the three-syringe pump flow reactor.

Flowrate $Co(AcO)_2$ / ml min^{-1}	Flowrate H_4L/KOH / ml min^{-1}	Flowrate Paraffin / ml min^{-1}	Temp. / °C	Time / min
0.740	0.740	1.480	50	5
0.987	0.493	1.480	50	5
0.493	0.987	1.480	50	5
1.184	0.296	1.480	50	5
1.316	0.164	1.480	50	5
0.370	0.370	0.740	50	10
0.493	0.247	0.740	50	10
0.247	0.493	0.740	50	10
0.592	0.148	0.740	50	10
0.658	0.082	0.740	50	10
0.247	0.247	0.493	50	15
0.329	0.164	0.493	50	15
0.164	0.329	0.493	50	15
0.394	0.099	0.493	50	15
0.438	0.055	0.493	50	15

0.740	0.740	1.480	70	5
0.987	0.493	1.480	70	5
0.493	0.987	1.480	70	5
1.184	0.296	1.480	70	5
1.316	0.164	1.480	70	5
0.370	0.370	0.740	70	10
0.493	0.247	0.740	70	10
0.247	0.493	0.740	70	10
0.592	0.148	0.740	70	10
0.658	0.082	0.740	70	10
0.247	0.247	0.493	70	15
0.329	0.164	0.493	70	15
0.164[a]	0.329	0.493	70	15
0.394	0.099	0.493	50	15
0.438	0.055	0.493	50	15

[a] This reaction produced the most crystalline and phase pure STA-12(Co), which is further analysed in this work. This is equivalent to a reaction ratio of 1:2:4 ($Co(AcO)_2$:H_4**L**:KOH).

Table S6.2. Summary of conditions tested for the synthesis of STA-12(Ni) using the three-syringe pump flow reactor.

Flowrate $Ni(AcO)_2$ / ml min^{-1}	**Flowrate H_4L/KOH / ml min^{-1}**	**Flowrate Paraffin / ml min^{-1}**	**Temp. / °C**	**Time / min**
0.740	0.740	1.480	70	5
0.987	0.493	1.480	70	5
0.493	0.987	1.480	70	5
1.184	0.296	1.480	70	5
0.370	0.370	0.740	70	10
0.493	0.247	0.740	70	10
0.247	0.493	0.740	70	10
0.592	0.148	0.740	70	10
0.247	0.247	0.493	70	15
0.329	0.164	0.493	70	15
0.164	0.329	0.493	70	15
0.394	0.099	0.493	70	15
0.123[a]	0.123	0.247	70	30
0.082	0.164	0.247	70	30

[a] This reaction produced the most crystalline and phase pure STA-12(Ni), which is further analysed in this work. This is equivalent to a reaction ratio of 1:1:2 ($Ni(AcO)_2$:H_4**L**:KOH).

S6.1.3 Synthesis of STA-12(Cd)

A syringe charged with a 0.1 mol dm^{-3} aqueous solution of cadmium(II) acetate was connected to a two pump configured flow reactor (V_Σ = 14.80 ml). The pumping rates of the pumps were set such that the ratio of reagents was 1:1:2 ($Cd(AcO)_2$:H_4**L**:KOH). For this synthesis, the reactor was heated to 70°C. Different pumping rates were used to give different reaction times (summarised in Table S6.3). The product was collected and separated by a sequence of centrifugation and washing with water and then ethanol.

Table S6.3. Flowrates of individual pumps and overall flowrate for different reaction time syntheses of STA-12(Cd). Reactions performed at 70°C

$Cd(AcO)_2$ Flowrate / ml min^{-1}	H_4L/KOH Flowrate / ml min^{-1}	Total Flowrate / ml min^{-1}	Reaction Time / min
1.48	1.48	2.96	5
0.74	0.74	1.48	10
0.49	0.49	0.98	15
0.37	0.37	0.74	20

Powder X-ray diffraction (PXRD) patterns of the products obtained after a reaction time of 5, 10, 15 and 20 min (Fig. S6.1) demonstrate that STA-12(Cd) may be obtained in pure form and with good crystallinity after just 5 minutes; a reaction time of 2 min yielded insufficient solids to collected a PXRD pattern. With increasing reaction times, the peaks appear narrower and more well-defined (for example the (140) reflection, highlighted in the dashed box) and furthermore, it becomes possible to resolve features at higher angles. The observations indicate that using our flow reactor set-up we are able to follow the growth and increase in long-range order of crystallites.

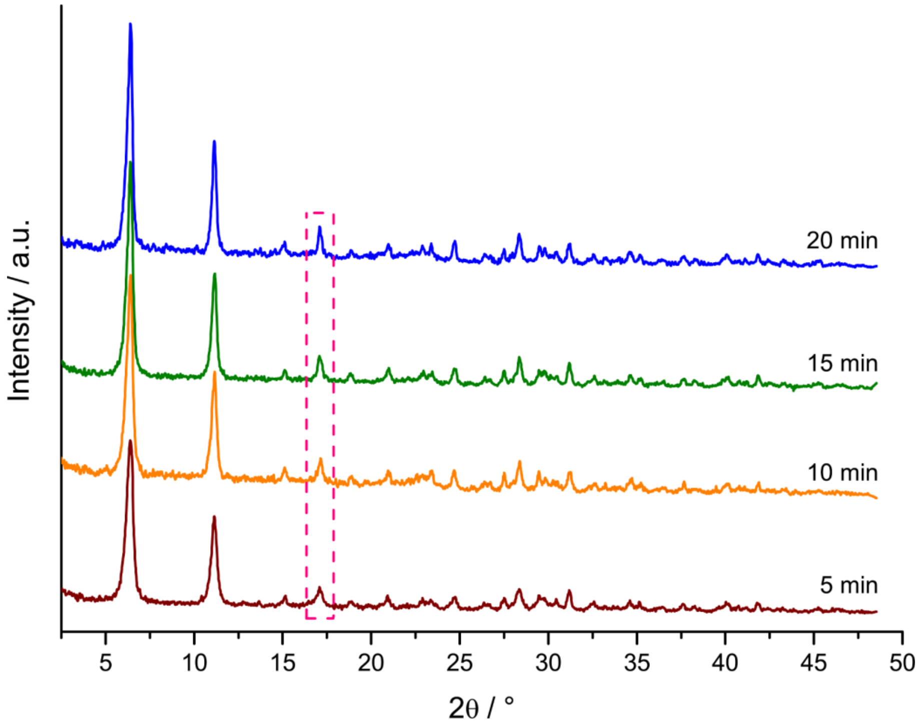

Figure S6.1. Laboratory PXRD patterns (λ = Cu K_α) of samples of STA-12(Cd) prepared in the flow reactor with reaction times increasing from 5 to 20 minutes. Dashed box indicates the (140) reflection, which narrows with increasing reaction time, indicating an increase in particle size.

S6.2 Structural Analysis of STA-12(Cd)

S6.2.1 Details of the Rietveld Refinement

Laboratory powder X-ray diffraction data were collected using a Stoe Stadi P diffractometer fitted with a Cu $K_{\alpha1}$ tube radiation source and a Mythen detector, in a transmission geometry. All stages of the refinement, including indexing, Pawley fitting and Rietveld refinement were performed using the routines of TOPAS-Academic V5.[18] The data were indexed with a metrically trigonal/hexagonal unit cell (a = b 27.4134 Å c = 6.7264 Å, GOF = 49.77) and found to have systematic absences consistent with the space group $R3$. STA-12 has been reported in the space group $R\bar{3}$ and thus this space group was selected for the subsequent Pawley fit. The cell refined to a = b =27.4087(11) Å c = 6.7275(3) Å in this space group, with an R_{wp} = 5.61 % and χ^2 = 1.145.

A Rietveld refinement was then performed using the structure of as-prepared STA-12(Mn) as a starting model[17] and the background, profile and unit cell parameters from the Pawley fit. Bonding restraints were applied to the octahedral Cd-O, Cd-O100 and Cd-N distances (all 2.35 Å); tetrahedral P-O and P-C distances (1.51 Å and 1.85 Å respectively); and the C-C and C-N bonds (1.53 Å and 1.51 1.53 Å). Additionally, through-space restraints were applied to the linker N···N, C···C (diagonal, cross-ring) and C···C (2nd neighbor) (2.91 Å, 2.91 Å and 2.48 Å respectively). The framework was fully refined, whilst the positions of the O atoms representing physisorbed water molecules in the channel were left unaltered from the Mn^{2+} structure. The channel O atoms were then removed and new positions were identified by Fourier mapping, revealing four sites. The occupancies and positions of these sites were then refined against the data, with an additional anti-bumping restraint applied to ensure O atoms remained at chemically reasonable separations (2.5 Å). Further cycles of refinement were performed with the framework and a final fit to the data of R_{wp} = 6.43 % and χ^2 = 1.302 was achieved. Rietveld plots for the final refinement are given in Fig. S6.2 and the final structural model viewed is shown in Fig. S6.3. Full crystallographic details are given in Table S6.4.

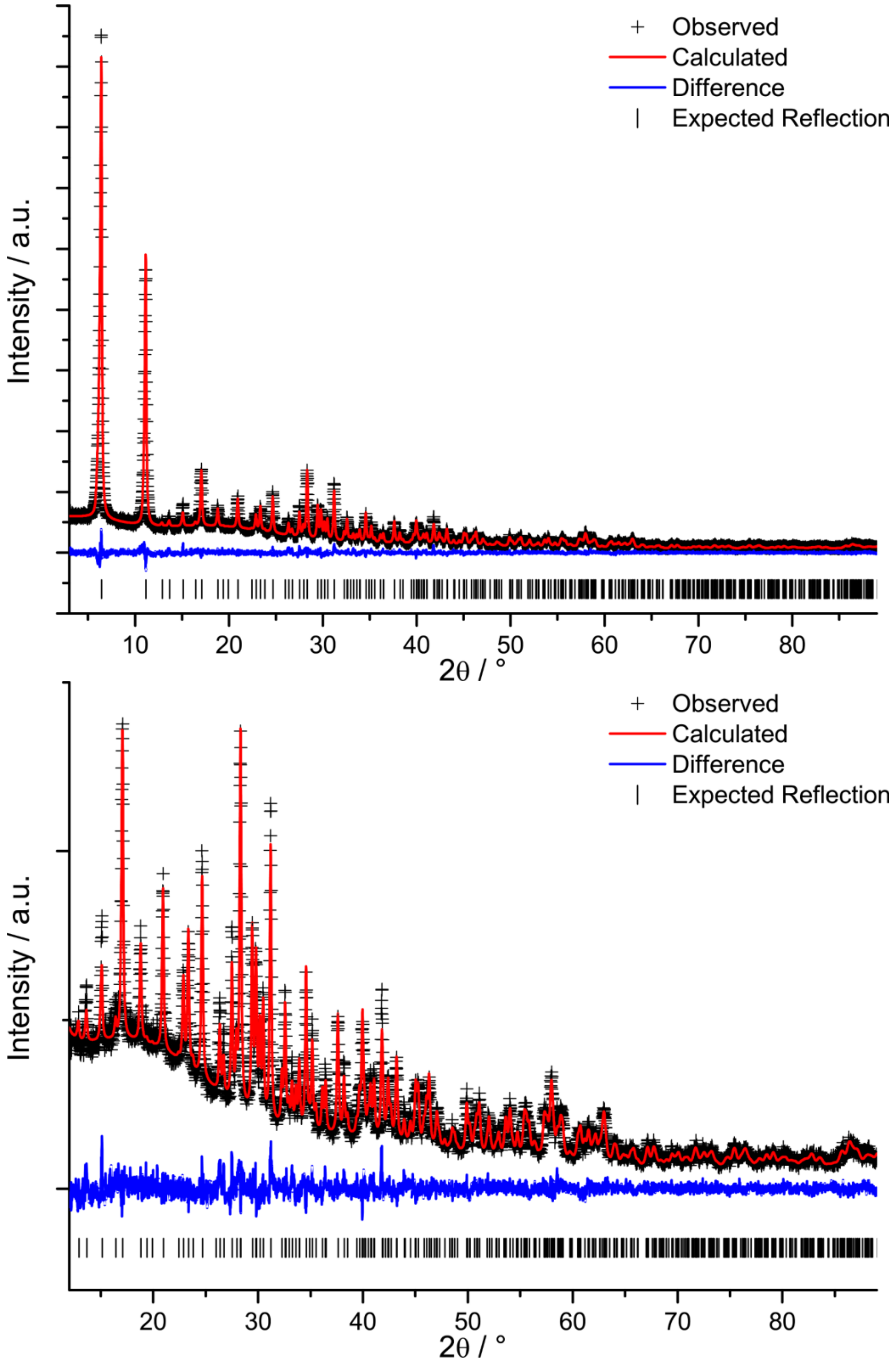

Figure S6.2. Rietveld plots for the final refinement of STA-12(Cd) showing the ranges 3-90° 2θ (top) and 12-90° 2θ (bottom). (Data collected using a laboratory Stoe Stadi P diffractometer fitted with a Cu $K_{\alpha1}$ tube radiation source).

S6.2.2 Structure of STA-12(Cd)

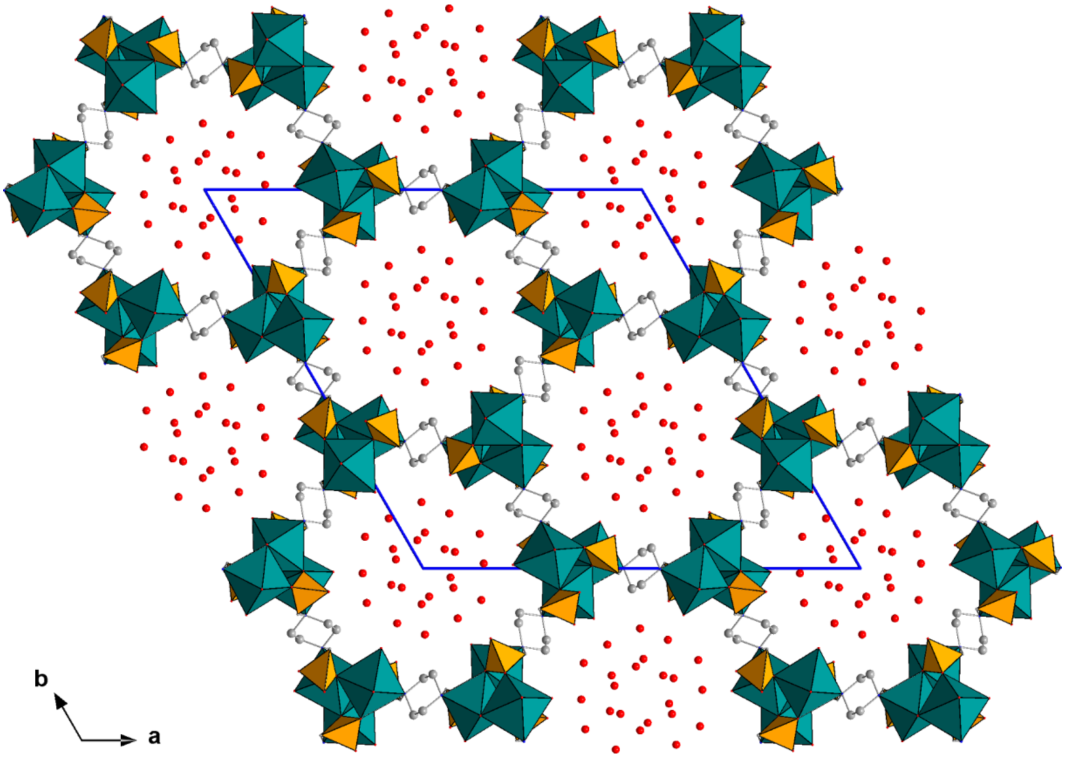

Figure S6.3. Structure of as-prepared STA-12(Cd), showing the honeycomb arrangement of heaxagonal unidirectional channels. Edge-sharing CdO_5N octahedra are bridged together by PO_3C phosphonate tetrahedra to form helical metal-phosphonate chains parallel to the *c*-axis. Chains are linked through piperazinyl groups, bonded to the phosphonate groups, which also coordinatively bond to the Cd^{2+} ions through their N atoms. (CdO_5N octahedra – turquoise; PO_3C tetrahedra – orange; C – gray spheres; water molecules (represented as O atoms) – red spheres.

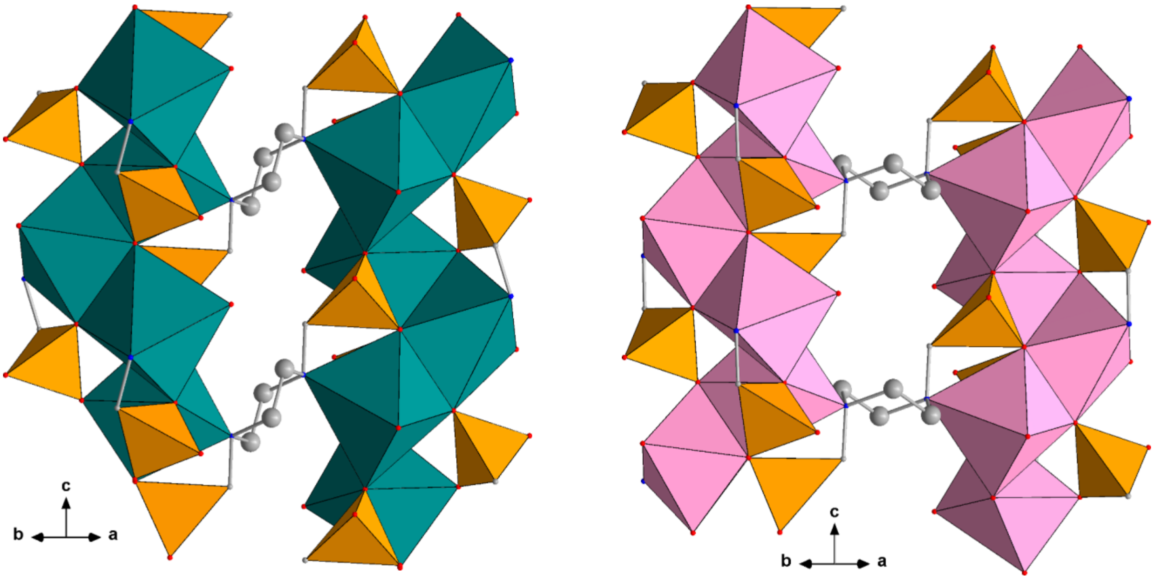

Figure S6.4. Structures of the chains of STA-12(Cd) (left) and STA-12(Mn) (right).[17] Both compounds have similar edge-sharing helical chains, however due to the greater radius of Cd^{2+} (Cd^{2+}: 1.10 Å; Mn^{2+}: 0.96 Å)[19], the piperazinyl groups are forced to lie parallel to the chains.

S6.2.3 Table of Crystallographic Data for STA-12(Cd)

Table S6.4. Crystallographic data for STA-12(Cd).

Compound	STA-12(Cd)
Empirical Formula	$[Cd_2(H_2O)_2(C_6H_{12}N_2O_6P_2)]\cdot5.52H_2O$
Moiety (refined, no H)	$CdC_3NO_{6.76}P$
Moiety Formula Weight	301.63
Calculated Density (no H) / g cm^{-3}	2.060
Space Group	$R\bar{3}$
Cell Setting	Trigonal
a / Å	27.4100(8)
c / Å	6.7279(2)
V / Å^3	4377.5(3)
Z	18
Diffractometer	Stoe Stadi P
Temperature / K	298
Wavelength / Å	Cu $K_{\alpha1}$
No. Reflections	778
No. Atoms	14
No. Restraints	21
R_p	0.0493
R_{wp}	0.0643
χ^2	1.302
R_{Bragg}	0.0156

S6.3 STA-12(Cd): Thermal & Elemental Analysis

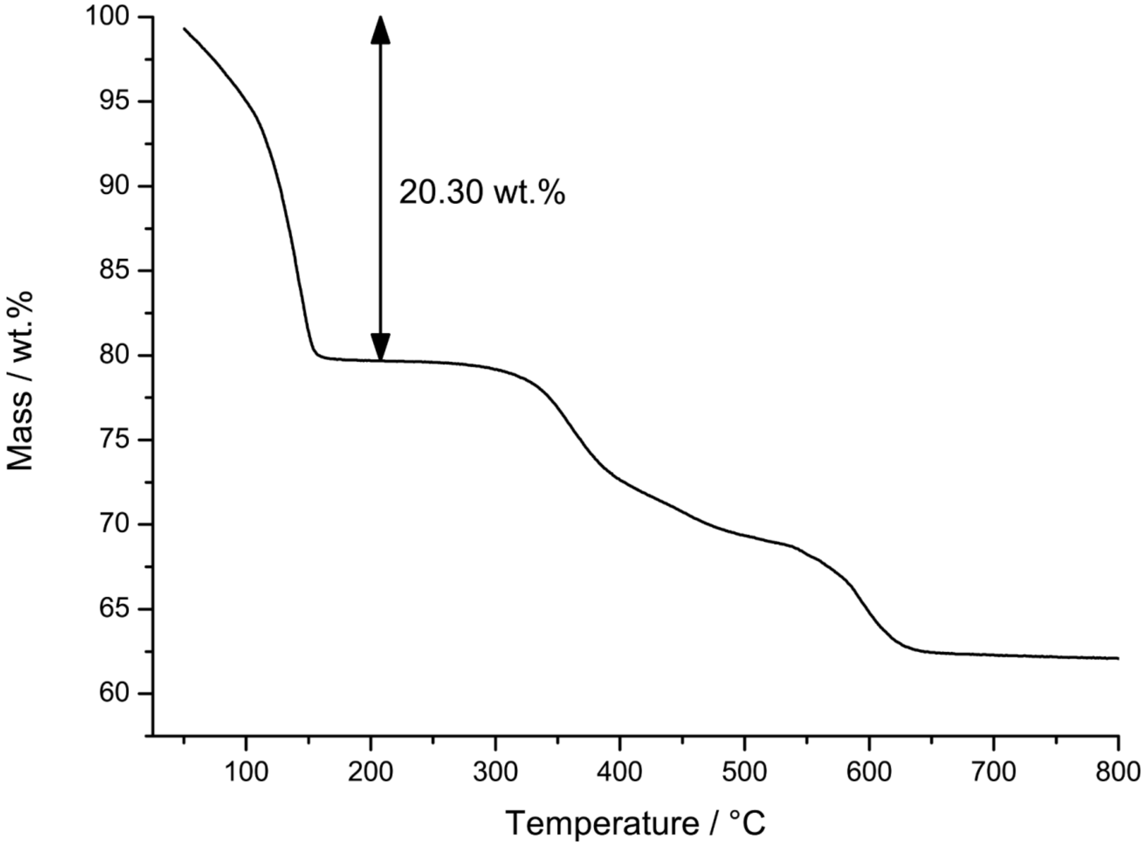

Figure S6.5. TGA Plot for STA-12(Cd) showing the principal weight loss event occurring on dehydration, assigned to the loss of both physisorbed and chemisorbed water molecules (14.9 wt.%; expected 15.4 wt.%). The dehydrated structure is stable to 315°C, above which temperature the structure collapses.

Table S6.5. Elementary analysis of STA-12(Cd) compared to the expected values for the theoretical compound of $[Cd_2(H_2O)_2(C_6H_{12}N_2P_2O_6)]{\cdot}5H_2O$.

	C %	**H %**	**N %**
Found	12.1	4.1	4.9
Expected	11.9	4.3	4.6

EDX measurements indicate a Cd^{2+}:P ratio of 1:1, which is in good agreement with the proposed composition of $[Cd_2(H_2O)_2(C_6H_{12}N_2P_2O_6)]{\cdot}5H_2O$.

S6.4 STA-12(Cd): Infrared Spectrum

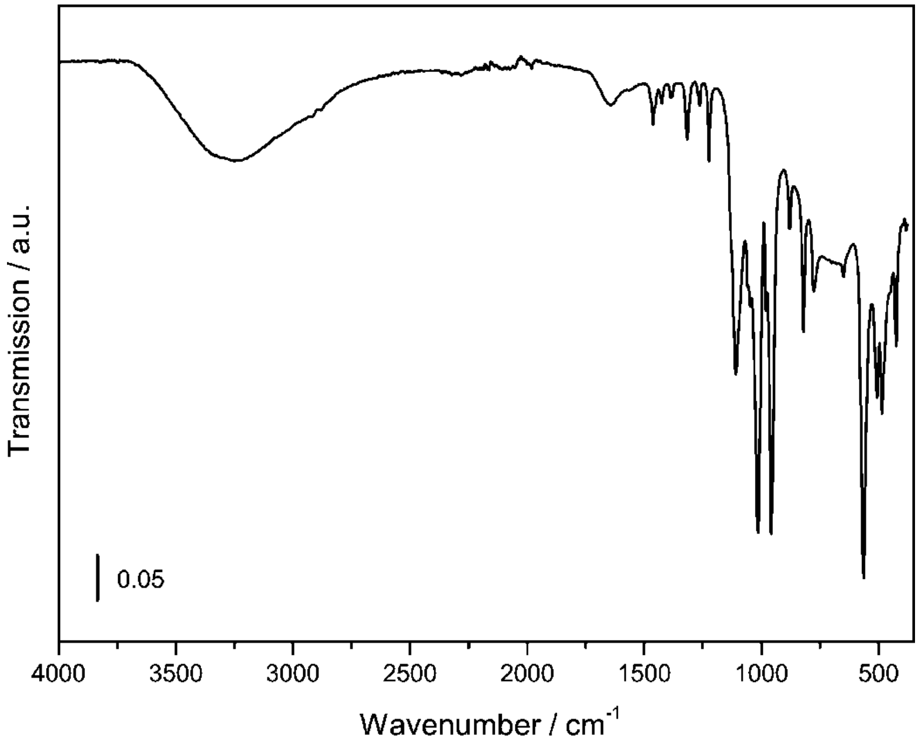

Figure S6.6. FTIR spectrum of STA-12(Cd). $\tilde{\nu}$ (cm^{-1}) = 3280 (b, O-H stretch – H_2O), 1465 (w, asymmetric CH_2 deformation - piperazine), 1377 (w, symmetric CH_2 deformation – piperazine), 1102 (s, asymmetric P-O), 958 (s, symmetric. P-O).

S6.5 STA-12(Cd): SEM Image

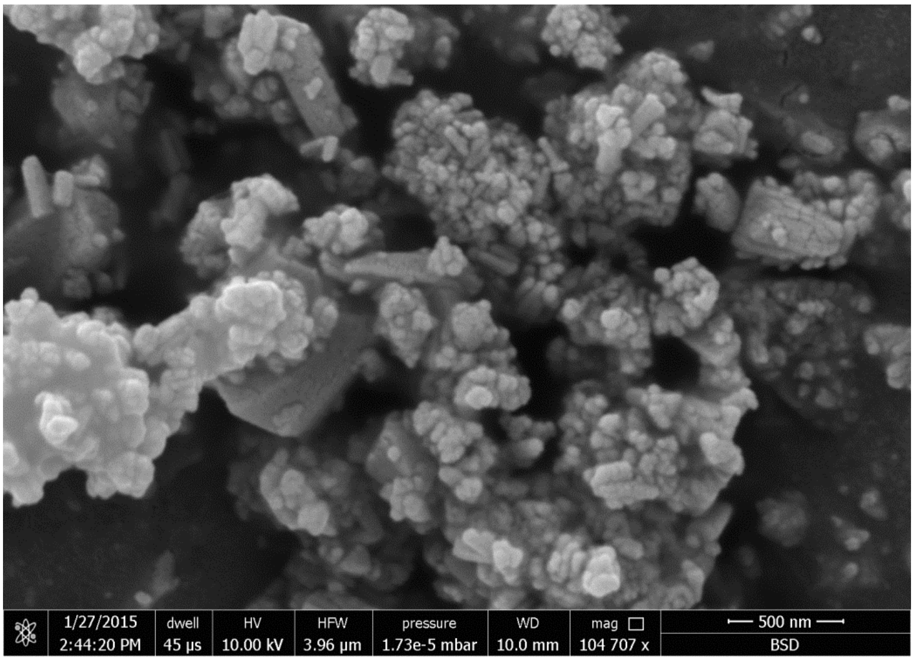

Figure S6.7. SEM micrograph of STA-12(Cd) produced using the flow reactor. Particles show no distinct form.

S6.6 STA-12(Cd): N_2 Sorption Experiments

STA-12(Cd) was activated for sorption measurements by heating the sample to 200°C under vacuum overnight. STA-12(Cd) is porous to N_2 at 77 K (Fig. S6.8) with a BET surface area (calculated over the range $p/p_0 = 0.033$-0.239) was determined to be 134(2) $m^2 g^{-1}$ and the micropore volume 0.08 $cm^3 g^{-1}$ (calculated by the Dubinin-Radushkevitch – D-R – method).[15] These values are significantly lower than for other members of the STA-12 family and even allowing for the greater mass of the Cd^{2+} cation, the micropore uptake calculated by the D-R method ($N_0 = 2.29(1)$ mmol g^{-1} is approximately 25 % less than expected. This indicates that there is some degree of pore blocking or an amorphous second phase in the analysed sample, possibly X-ray amorphous cadmium hydroxide. The lower N_2 porosity is not attributed to a collapse of the framework during activation, since PXRD patterns before and after the activation procedure show no changes (Fig. S6.9.)

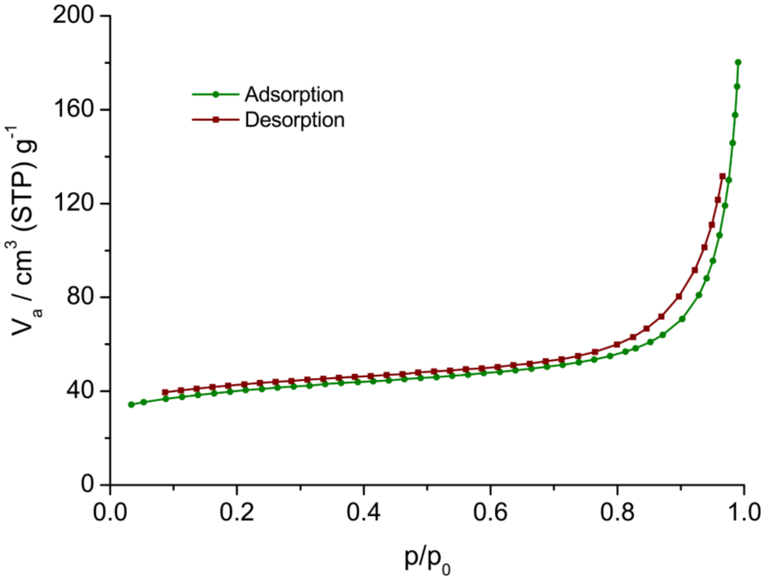

Figure S6.8. N_2 adsorption and desorption isotherms for STA-12(Cd) measured at 77 K.

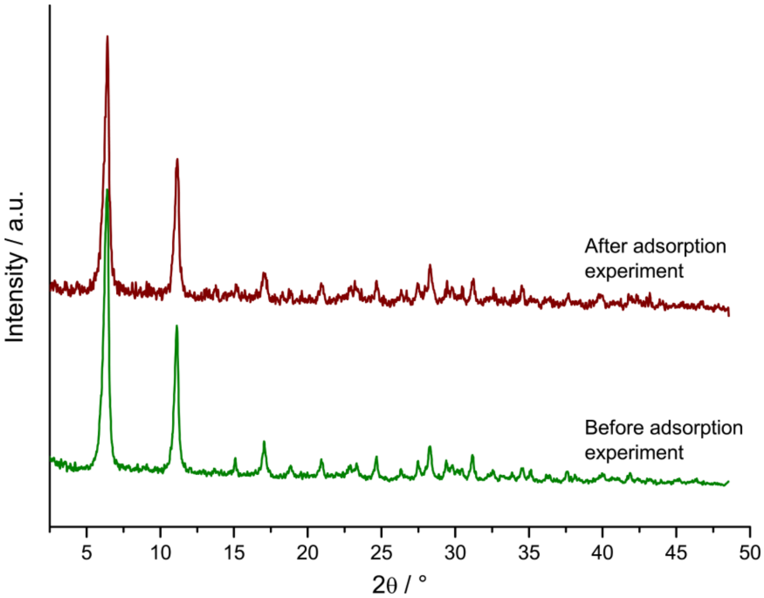

Figure S6.9. PXRD patterns (λ = Cu $K_{\alpha 1}$) for STA-12(Cd) before and after activation for the N_2 sorption experiment.

S7 References

1 M. Gimeno-Fabra, A. S. Munn, L. A. Stevens, T. C. Drage, D. M. Grant, R. J. Kashtiban, J. Sloan, E. Lester and R. I. Walton, *Chem. Commun.*, 2012, **48**, 10642–10644.

2 K.-J. Kim, Y. J. Li, P. B. Kreider, C.-H. Chang, N. Wannenmacher, P. K. Thallapally and H.-G. Ahn, *Chem. Commun.*, 2013, **49**, 11518–11520.

3 M. Faustini, J. Kim, G.-Y. Jeong, J. Y. Kim, H. R. Moon, W.-S. Ahn and D.-P. Kim, *J. Am. Chem. Soc.*, 2013, **135**, 14619–14626.

4 P. A. Bayliss, I. A. Ibarra, E. Perez, S. Yang, C. C. Tang, M. Poliakoff and M. Schroder, *Green Chem.*, 2014, **16**, 3796–3802.

5 M. Rubio-Martinez, M. P. Batten, A. Polyzos, K.-C. Carey, J. I. Mardel, K.-S. Lim and M. R. Hill, *Sci. Rep.*, 2014, **4**.

6 L. Paseta, B. Seoane, D. Julve, V. Sebastián, C. Téllez and J. Coronas, *ACS Appl. Mater. Interfaces*, 2013, **5**, 9405–9410.

7 P. M. Schoenecker, G. A. Belancik, B. E. Grabicka and K. S. Walton, *AIChE J.*, 2013, **59**, 1255–1262.

8 L. D'Arras, C. Sassoye, L. Rozes, C. Sanchez, J. Marrot, S. Marre and C. Aymonier, *New J. Chem.*, 2014, **38**, 1477–1483.

9 J. P. S. Mowat, J. A. Groves, M. T. Wharmby, S. R. Miller, Y. Li, P. Lightfoot and P. A. Wright, *J. Solid State Chem.*, 2009, **182**, 2769–2778.

10 M. J. Cliffe, W. Wan, X. Zou, P. A. Chater, A. K. Kleppe, M. G. Tucker, H. Wilhelm, N. P. Funnell, F.-X. Coudert and A. L. Goodwin, *Nat Commun*, 2014, **5**, 4176.

11 L. Valenzano, B. Civalleri, S. Chavan, S. Bordiga, M. H. Nilsen, S. Jakobsen, K. P. Lillerud and C. Lamberti, *Chem. Mater.*, 2011, **23**, 1700–1718.

12 G. C. Shearer, S. Chavan, J. Ethiraj, J. G. Vitillo, S. Svelle, U. Olsbye, C. Lamberti, S. Bordiga and K. P. Lillerud, *Chem. Mater.*, 2014, **26**, 4068–4071.

13 A. Schaate, P. Roy, A. Godt, J. Lippke, F. Waltz, M. Wiebcke and P. Behrens, *Chem. – Eur. J.*, 2011, **17**, 6643–6651.

14 F. Niekiel, M. Ackermann, P. Guerrier, A. Rothkirch and N. Stock, *Inorg. Chem.*, 2013, **52**, 8699–8705.

15 F. Rouquerol, J. Rouquerol and K. S. W. Sing, *Adsorption by Powders and Porous Solids: Principles, Methodology and Applications*, Academic Press, 1998.

16 J. A. Groves, S. R. Miller, S. J. Warrender, C. Mellot-Draznieks, P. Lightfoot and P. A. Wright, *Chem. Commun.*, 2006, 3305–3307.

17 M. T. Wharmby, G. M. Pearce, J. P. S. Mowat, J. M. Griffin, S. E. Ashbrook, P. A. Wright, L.-H. Schilling, A. Lieb, N. Stock, S. Chavan, S. Bordiga, E. Garcia, G. D. Pirngruber, M. Vreeke and L. Gora, *Microporous Mesoporous Mater.*, 2012, **157**, 3–17.

18 A. Coelho, *TOPAS-Academic v5*, Coehlo Software, Brisbane, Australia, 2012.

19 R. D. Shannon, *Acta Crystallogr. Sect. A*, 1976, **32**, 751–767.